Fluence Effects in C_{60} Cluster Bombardment of Silicon†

Kristin D. Krantzman*,‡ and Andreas Wucher§

Department of Chemistry and Biochemistry, College of Charleston, Charleston, South Carolina, 29424, and Faculty of Physics, University Duisburg-Essen, 47048 Duisburg, Germany

Received: June 28, 2009; Revised Manuscript Received: October 11, 2009

Ⓦ **This paper contains enhanced objects available on the Internet at http://pubs.acs.org/JPCC.**

In this theoretical investigation, we combine the results of molecular dynamics (MD) simulations with a simple statistical sputtering model (SSM) in order to understand the factors limiting the optimum depth resolution achievable in sputter depth profiling experiments. The advantage of the SSM model is that it can be used to extrapolate the MD simulations toward the regime of high projectile fluence. First, a recently developed scheme [Russo, M. F., Jr.; Postawa, Z.; Garrison, B. J., *J. Phys. Chem. C* **2009**, *113*, 3270] is adapted to calculate 200 cumulative impacts of 20-keV C_{60} bombardment on a Si substrate, which corresponds to a projectile fluence of 3.5×10^{13} cm^{-2}. The following results are studied as a function of fluence: the development of surface topography, the amount and depth of origin of sputtered material, and the relocation of substrate particles, which produces interlayer mixing. Data from the MD simulations are used as input parameters in the SSM, which is able to reproduce results consistent with the MD simulations. A major finding from these studies is that the statistical nature of the sputtering process has a significant effect on the achievable depth resolution. The optimum delta layer response width for Si is estimated to be about 3 nm, while corresponding values of the order of 10 nm are predicted for molecular systems.

1. Introduction

The interaction of cluster ion beams with solid surfaces has recently become of great interest because these projectiles open the door to molecular sputter depth profiling applications. In this type of experiment, a solid surface is eroded by an ion beam, while the composition of the momentarily exposed surface is studied using a surface sensitive method for chemical analysis. Prominent examples of such a technique are mass spectrometric surface analysis methods such as secondary ion or neutral mass spectrometry (SIMS/SNMS), where the sputtered material released from the surface under ion bombardment is analyzed in terms of its chemical composition. An important feature of these methods is the fact that the flux of sputtered particles contains not only atoms but also molecules which may be more or less characteristic of the molecular surface structure. For many years, it was common knowledge that this molecular information was rapidly quenched under ion bombardment if projectile ion fluences beyond the so-called static limit were accumulated at the surface. In principle, the respective fluence limit must be defined to ensure that the probability for the same surface area being influenced by more than one projectile impact is negligible. In practice, only a small fraction of a monolayer must be removed from the surface, a condition which obviously prevents sputter depth profiling.

While the above situation is practically always true under bombardment with atomic ions, it has been discovered that the use of cluster projectile ions instead of atomic ions may allow the use of larger ion fluences far beyond the static limit without destroying the molecular integrity of the sample.[1] The general philosophy behind this observation is that a cluster projectile deposits its impact energy into a shallower subsurface region, where it can be more efficiently utilized for sputtering.[2] These projectiles simultaneously deliver many low-energy atoms to the surface, thereby minimizing impact induced mixing, while concurrently maintaining a large enough total projectile energy for the formation of a finely focused ion beam.[2] For the specific case of a 20-keV C_{60} cluster, the energy per impinging C atom is comparable to the low energies necessary for high depth resolution. Due to the recent availability of commercial equipment delivering high-quality C_{60} ion beams,[3] sputter depth profiling[4−23] or even, in combination with laterally resolved imaging techniques, three-dimensional chemical analysis of molecular samples has become feasible.[14,24−30]

For many years, mass spectral sputter depth profiling has been an essential analytical tool in the semiconductor industry. In this field, SIMS is being extensively used to determine, for instance, dopant profiles in semiconductors with high sensitivity and depth resolution. In particular, the steadily decreasing junction depth has led to ever increasing requirements regarding the depth resolution of such an analysis, with today's ultrashallow dopant profiles requiring the ability to resolve structures with only a few monolayers thicknesses. A prominent strategy to judge a method's ability to provide the depth resolution needed for such an analysis is to measure the response to a thin marker layer embedded into the semiconductor crystal. Ideally, the marker should be a single monolayer of dopant material (which will in the following be called a "delta layer"), since the response function measured for such a marker directly yields the depth resolution of the profiling method. Experiments performed on such structures with either atomic (Cs^+) or molecular (O_2^+) projectile ions have revealed apparent marker widths to decrease with decreasing impact energy reaching values of the order of 1 nm at energies of several 100 eV.[31] In

† Part of the "Barbara J. Garrison Festschrift".

* To whom correspondence should be addressed. E-mail: krantzmank@cofc.edu.

‡ College of Charleston.

§ University Duisburg-Essen.

10.1021/jp906050f
Published on Web 12/08/2009

this context, particular attention has been paid to the use of cluster ion beams as erosion tools.[14,32−35]

Attempts have been made to employ C_{60} ion beams for high resolution sputter depth profiling of inorganic samples. A particularly successful example was found for metallic multilayer structures, where the profiles obtained with 20-keV C_{60}^+ ions exhibit a significantly improved depth resolution compared to atomic projectiles.[14,34] Application of 15-keV C_{60}^+ to an As delta doped structure in Si revealed marker widths of the order of 6 nm, which are, however, by roughly a factor of 2 larger than those obtained with 500-eV Cs^+ ions.[32] In view of the similar impact energy per atom in both cases, this difference was attributed to the development of surface topography under ion bombardment.

A unique set of problems was discovered in depth profiling experiments of Si with C_{60}^+.[32] At low incident energies below a threshold value of ∼12 keV, carbon deposition exceeds the sputter rate. At kinetic energies above this value, a sputtering yield is observed, but the sputtering rate steadily decreases as carbon builds up on the surface. At high incident energies, the deposited carbon produces unusual topographical features on the surface. Similar effects have also been observed during large-scale depth profiling of some organic materials.[36,37]

In an attempt to interpret the puzzling experimental results, molecular dynamics (MD) simulations have been performed to model the impact of energetic C_{60} clusters onto a single crystal Si surface.[38,39,41] The simulations show that projectile-induced surface chemistry occurs in this particular case because of the formation of strong covalent bonds between the C and Si atoms, which result in nearly all of the C atoms remaining embedded in the surface after bombardment. The experimentally observed transition from net deposition to net erosion at energies around 12 keV was nicely reproduced by the MD results. In addition, similar studies have been performed on SiC, diamond, and graphite surfaces, all of which contain substrate atoms that can form bonds with C atoms from the projectile.[40,42] A fundamental drawback of these calculations, however, is that they are static in the sense that each projectile is assumed to impinge onto a virgin, undisturbed crystal surface. Only effects occurring in the course of single impact events can be studied, and cumulative effects relevant to depth profiling experiments cannot be treated by traditional static MD simulations.

In the present work, we have therefore adopted a recently developed strategy[43] to expand MD simulations to projectile fluences beyond the static limit. The objective of the simulations reported here is to obtain a conceptual picture on a microscopic scale of the principal processes occurring during multi-impact bombardment along with their implications with respect to sputter depth profiling. In this first report, we will show that it is possible to simulate the onset of surface topography formation, atom relocation, and interlayer mixing that occurs during accumulation of ion fluences that are large enough to remove several monolayer equivalents of the bombarded sample. C atoms are incorporated into the sample as a result of each impact. However, at this fluence, the C atoms compose only 1.4% of the total atoms in the substrate. Therefore, many more impacts are needed to build up a substantial enough C concentration to study the effects of Si−C chemistry.

In spite of the success of the multiple-impact MD simulations, it is clear that this approach will not be able to model ion fluences that are necessary to remove hundreds of monolayers or more. In order to be able to describe a realistic sputter depth profile, it is therefore necessary to develop strategies to extrapolate the MD results toward larger fluences by means of simple model calculations. Ideally, one would try to develop a phenomenological model with input parameters that are derived from the initial-stage MD calculations. A similar strategy has already been used earlier to predict sputter yields under cluster ion bombardment by means of both the MEDF model[44] and the quadratic friction model.[45] In the same spirit, we introduce a simple statistical sputtering model (SSM) to describe the essential features of bombardment-induced microtopography formation, sputter removal, and interlayer mixing, which are all necessary to understand a sputter depth profile. It is shown that the SSM is capable of quantitatively reproducing the MD results in a consistent manner, i.e., predict relevant trends calculated by MD using input parameters that are derived solely from other parts of the MD data itself. Using the model to extrapolate to larger fluence then enables us to predict the delta layer marker width as one of the key parameters of a sputter depth profile.

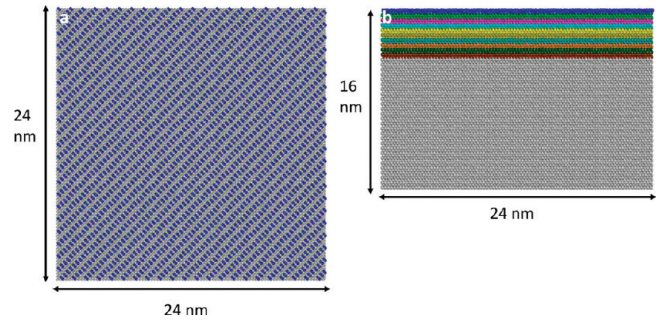

Figure 1. Initial model system of the entire sample: (a) Top view illustrating Si dimers (blue). (b) Side view showing the color scheme for the top ten layers of Si atoms.

2. Molecular Dynamics Simulations

a. Description of the Simulations. The simulations use a "divide and conquer" scheme developed by Russo et al.,[43] which outlines a protocol treating multiple projectile impacts onto the same surface area. The classical method of MD simulations is used to describe the motion of atoms during each single bombardment event, and the application of this method to the keV bombardment of solids is explained comprehensively elsewhere in the literature.[46,47] Briefly, the position and velocity of each atom as a function of time is determined by numerically integrating Hamilton's equations of motion. The force on each atom is calculated from the gradient of the potential energy function used to describe the interactions between atoms.

An empirical many body potential developed by Tersoff is used to model the Si−Si, C−C, and Si−C interactions.[48] The empirical parameters in the potential are fit to the energetics and structure of Si, diamond, and SiC. The Tersoff potential is not sufficiently repulsive at short distances, thus an exponential spline function is used to smoothly connect the Ziegler, Biersack, and Littmark (ZBL)[49] potential with the two-body Tersoff Si−Si, C−C, and Si−C potentials.[50]

The entire silicon surface is modeled by a Si{100} crystal with dimensions of 24 nm × 24 nm × 16 nm containing 511104 atoms arranged in 66 layers of 7744 atoms and is shown in Figure 1. The top layer of Si atoms are placed in the (2 × 1) reconstruction and the entire surface is then relaxed and equilibrated at 0 K using an algorithm based on the generalized Langevin equation (GLE). The positions of the Si dimers on the surface are shown in the top view, while the side view illustrates the color scheme used to represent the top ten monolayers of Si. Each monolayer defined this way has a

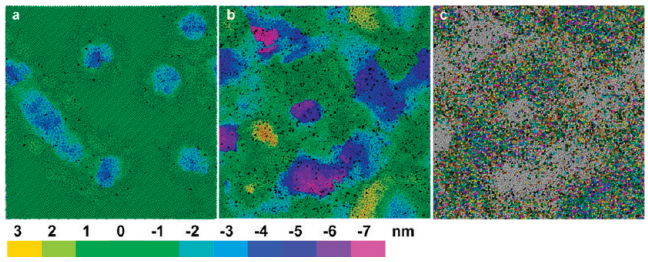

Figure 2. Top view of entire sample with atoms colored by height or original layer for different fluences: (a) Height distribution of the visible Si atoms after ten impacts. The color scheme is based on the vertical positions of the atoms from a depth of 7.0 nm below to 3.0 nm above the location of the original surface. (b) Same image as in a after 200 impacts. (c) Same image as in b with the Si atoms colored by original layer using same scheme shown in Figure 1b. The black points correspond to the positions of the deposited C atoms. (A MPG animation of Figure 2b depicting a top view of the atom positions colored by height after each of the 200 successive impacts is available as a Web-enhanced object).

thickness of $d_{layer} = 0.27$ nm, a value which is compatible with the statistical definition of $d_{layer} = n^{-1/3}$, with n being the atom density of Si. The same color scheme will be used to identify the different layers throughout the paper.

A set of 200 impact points is chosen randomly over the entire surface of the Si crystal, which corresponds to a total fluence of 35.2×10^{12} cm^{-2}. The trajectory for each impact is run using a smaller subsample extracted from the main crystal. Each local subsample is cylindrically shaped in order to reduce the number of atoms included in the calculation of the trajectory for each impact and is chosen to be sufficiently large to contain a single bombardment event. The subsample is centered at the impact point and periodic boundary conditions around the main sample are used when necessary. In order to achieve a larger fluence with a smaller number of impacts, the size of the entire sample is smaller than that used by Russo et al.[43] As a consequence, each one of the impacts has overlapping regions, and therefore, the trajectory for each impact was run successively.

In these simulations, the subsample used for each impact has a radius of 8.3 nm and a depth of 10 nm from the height of the original surface. The subsample is encased on the sides and bottom by a heat bath composed of a 2.0 nm region of stochastic atoms kept at 0 K by a frictional force, which is used to prevent energy induced by pressure waves being reflected from the boundary walls back into the sample.[2,51] The stochastic layer is enclosed by a 0.5 nm region of rigid atoms in order to maintain the original shape of the local sample so that it can be reinserted into the large sample without overlapping with the other atoms in the sample.[43] For each impact, the randomly oriented C_{60} projectile was placed at a sufficient distance above the surface that the interaction potential is negligible. The trajectory for each impact was run for 20 ps, which is sufficiently long for the completion of the bombardment event and re-equilibration of the sample back to a temperature of 0 K.

b. Results and Discussion. ***i. Surface Topography.*** As a starting point, the surface condition during the initial stages of bombardment is investigated at a fluence that corresponds to the experimental static limit. This is done by viewing a height distribution of the entire sample. In the remainder of this paper, the term "height" will be used to describe the coordinate z of atoms perpendicular to the original surface, with the zero point being defined at the position of the original surface. In Figure 2a, the atom positions colored by height are shown after ten impacts, which corresponds to a fluence of 1.8×10^{12} cm^{-2}. Craters surrounded by rims are formed near each impact point,

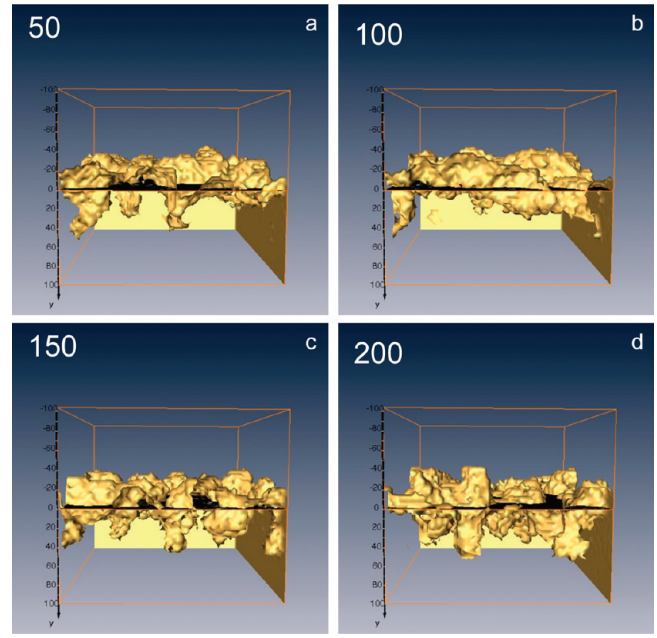

Figure 3. Isosurface representations of the momentary surface after accumulation of (a) 50, (b) 100, (c) 150, and (d) 200 projectile impacts (corresponding to projectile ion fluences of 8.8, 17.6, 26.4, and 35.2×10^{12} cm^{-2}, respectively). (Animations of the panels in Figure 3 are available as Web-enhanced objects: Video 1: top view of evolution of surface topography after each of the 200 successive impacts; video 2: cross sectional orthoslice moving across the surface in the x direction to visualize the surface topography after 50 impacts; video 3: same as in video 2 after 100 impacts; video 4: same as in video 3 after 150 impacts; and video 5: same as in 4 after 200 impacts).

and there is little overlap between the disturbed regions, which meets the criterion for the static limit. The condition of the surface at fluences below this point is used to extract static parameters for the statistical sputtering model, which is described later.

In Figure 2b, the height distribution of the Si atoms and the positions of the incorporated C atoms are shown after an accumulation of 200 impacts. The surface has been significantly altered from its original state and the height distribution of the Si atoms shows a large variance. There are now both mountains and valleys in the surface, and a complex surface topography has developed. Even though an equivalent of five monolayers of Si has been removed and the average height of the surface atoms has decreased, there is a significant buildup of material above the original surface up to a height greater than 3.5 nm. In addition, there is an erosion of material, with the formation of craters as deep as 8.0 nm below the original surface.

The same surface is shown Figure 2c, but the Si atoms are now colored by their initial positions in layers of the undisturbed crystal using the color scheme shown in Figure 1b. The majority of Si atoms have been dislocated from their original layers and the bombardment process results in both the removal and relocation of Si atoms. The gray regions show that atoms originally located below the tenth layer are now exposed at the surface. We can deepen our qualitative understanding of the changes in surface topography as a function of fluence by a three-dimensional visualization of the momentary surface at different fluences, which are shown in Figure 3. In each figure, the black plane slicing through the sample represents the original surface, and the surface coordinates (i.e., the height value of the uppermost atoms as a function of the lateral position) have been determined as described below. The visual pictures in Figure 3 show that the surface becomes uneven and bumpy upon

TABLE 1: Statistical Values Related to the Height Distribution of Atoms on the Surface As a Function of the Number of Impacts

number of impacts	projectile ion fluence (cm^{-2})	average height of uppermost Si atoms (nm)	root mean square of average height of uppermost Si atoms (nm)	monolayer equivalents removed	fraction of atoms from original top layer left in surface
0	0	−0.0905	0.04	0	0
10	1.76×10^{12}	−0.0349	0.90	0.34	0.89
50	8.81×10^{12}	−0.0107	1.67	1.24	0.71
100	17.6×10^{12}	−0.281	1.92	2.49	0.56
150	26.4×10^{12}	−0.551	1.97	3.61	0.46
200	35.2×10^{12}	−0.912	1.97	4.92	0.36

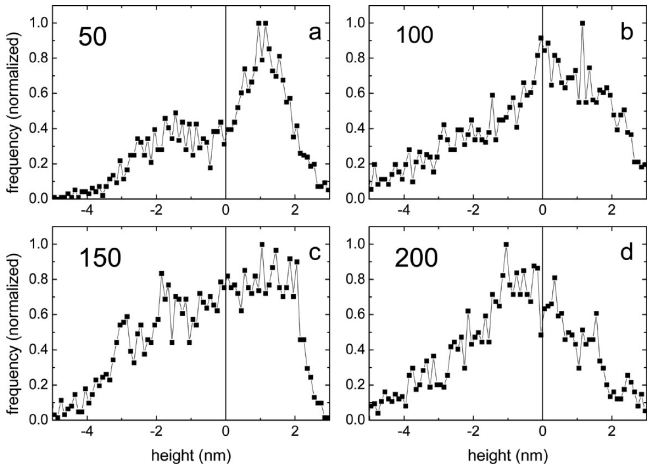

Figure 4. Statistical height distributions of the Si surface atoms determined after (a) 50, (b) 100, (c) 150, and (d) 200 projectile impacts (corresponding to projectile ion fluences of 8.8, 17.6, 26.4, and 35.2×10^{12} cm^{-2}, respectively).

bombardment. After only 50 impacts, protrusions above the original surface and cavities deep into the surface have developed. Details of the shape of these features can be seen from vertical slices through the isosurface as a function of lateral *x* or *y* positions, which are included as animations in Figure 3. As the fluence increases, the bumpiness of the surface and the number of cavities and protrusions increases. In addition, the heights of the protrusions and the depth of the cavities increase with fluence. The average heights of the Si atoms on the uppermost surface are listed in Table 1 at different fluences. During the initial stages of bombardment, the surface swells and the average height of the top Si atoms increases even though atoms are removed from the surface. The average height of the top Si surface atoms continues to increase and does not start to consistently decrease from the original height of the surface until an accumulation of 58 impacts or a projectile ion fluence of about 2×10^{12} cm^{-2}. After the final impact in the trajectory calculations (corresponding to a projectile ion fluence of 35×10^{12} cm^{-2}), the average height of the top Si atoms has decreased by 0.82 nm.

A quantification of the surface topography can be obtained by an analysis of the statistical height distribution as a function of fluence. The first step in this analysis is to divide the entire surface into square lateral cells and determine the height of the uppermost atom within each cell. This value defines the height coordinate of the momentary surface at the position of each cell. Next, the number of times the value of each surface height occurs is counted and the resulting frequency is plotted as a function of the surface height. The frequency distributions determined this way are shown in Figure 4 at different projectile fluences corresponding to the pictures in Figure 3. In order to allow a better comparison, the curves were normalized to maximum frequency.

Apparently, there is a significant change in the nature of the surface topography with fluence. After 50 impacts (Figure 4a), there is a bimodal distribution with maximum frequencies located both below and above the original surface. This finding can be understood as follows. As seen in Figure 1a, each impact onto the original undisturbed surface generates a crater surrounded by a rim of adatoms. The height distribution contributed by each crater peaks at the depth of the crater bottom, where the derivative of height with respect to the coordinates parallel to the surface naturally goes through zero. In the same way, each rim contributes a height distribution which peaks at the top of the rim. As seen in Figure 1a, all craters and rims have a similar shape, with a typical crater depth of 2−4 nm and rim height of 1−2 nm. In a situation like that shown in Figure 1a, where only part of the surface is covered by independent impact events, one would therefore expect a trimodal height distribution with maxima at +1..2, 2..4, and 0 nm (the latter corresponding to the yet undisturbed part of the original surface). If enough impacts have been accumulated such that the surface area is completely covered, the central maximum at height zero is expected to disappear, leaving a bimodal height distribution as shown in Figure 4a. Since not much material has been removed at that point, the integral under the positive and negative modes are roughly the same, indicating that material from craters reaching up to 4 nm below the surface has been relocated to crater rims at heights up to 2 nm above the surface. As the fluence increases, all following projectiles impinge onto a surface that has already been modified by one or more previous impacts. As a consequence, the bimodal height distribution becomes gradually washed out, because subsequent impacts will statistically hit somewhere between a rim top and a crater bottom, ultimately generating a purely statistical, unimodal distribution centered around the momentary average surface height. At the same time, the maximum frequency shifts to a lower height value because material is being removed from the surface. The distributions are still asymmetric, reflecting the fact that upward relocation of atoms is less efficient than downward relocation (as observed already in single impact craters). After 200 impacts, shown in Figure 3d, the height distribution develops a more Gaussian-like character.

In Table 1, the root-mean-square (rms) of the statistical height distribution, which is often defined as a measure of the surface roughness, is given at different fluences. It is seen that the rms roughness increases dramatically from 0.04 to 1.67 nm after 50 impacts, i.e. during accumulation of a fluence corresponding to about five times the static limit. Once 100 impacts (corresponding to a fluence of about 2×10^{13} cm^{-2}) have accumulated, the rms roughness has increased to 1.92 nm and this value then increases only slightly to 1.97 nm after 200 impacts.

ii. Sputter Removal. The number of monolayer equivalents (ML) of removed material is plotted as a function of fluence in Figure 5. It is found that the removal rate is approximately constant during the initial stages of depth profiling calculated

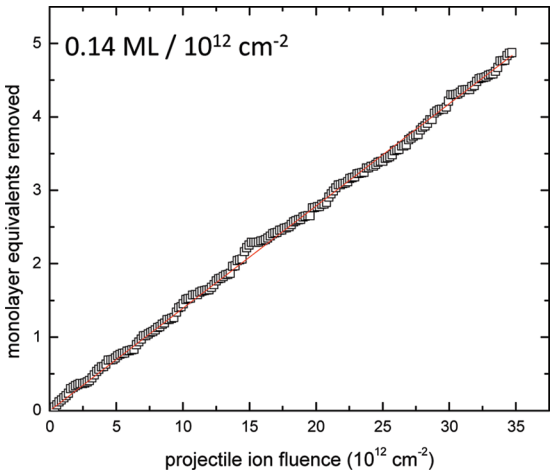

Figure 5. Number of monolayer equivalents removed from the sample by sputtering vs projectile ion fluence. Symbols: results of the MD simulation; straight line: linear fit.

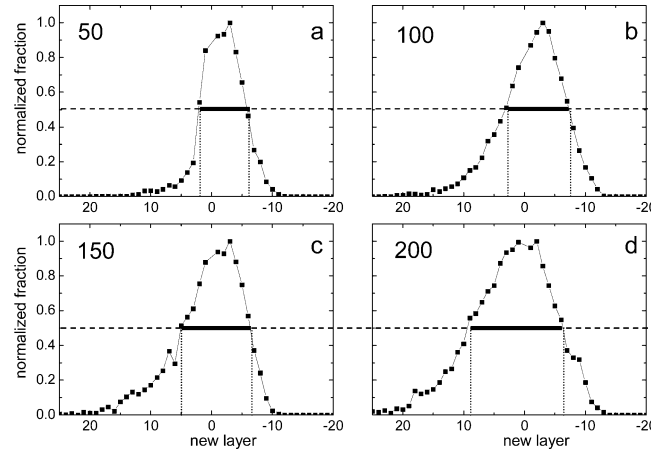

Figure 6. Distribution of vertical positions of atoms originally located in the uppermost layer after accumulation of (a) 50, (b) 100, (c) 150, and (d) 200 projectile impacts. Horizontal lines are drawn to illustrate the half-width of each distribution, which are equal to 8, 10, 12, and 15 monolayers, respectively. Originally defined layers below the surface have positive integer indices, while equivalent layers above the surface have negative integer indices.

in this paper for normal incidence bombardment of C_{60} on a Si surface. This finding is notable since it indicates that, at least for the system investigated here, the sputter yield does not significantly depend on the surface topography. From the linear fit indicated by the solid line in Figure 5, the removal rate is calculated to be 0.14 ML/10^{12} cm^{-2}. After 200 impacts, about 5 ML of material have been removed. Assuming the original atom density of the initial crystal, this would correspond to a layer of $5 \times d_{\text{layer}} = 1.36$ nm thickness, and one would therefore intuitively expect the average surface to have receded by that amount. Interestingly, the actual decrease in average height is only 0.82 nm, indicating an initial swelling of the crystal. Such an effect could in principle be related to the incorporation of carbon atoms from the projectile. Assuming the same volume per C and Si atom, the total number of implanted C atoms would make up for about 0.3 nm of the observed difference. Since the number density of SiC is about twice as large as that of Si, however, this value is likely to overestimate the actual effect. Apparently, the number density of Si atoms in the surface region must have decreased as a consequence of the relocation of material from below to above the original surface. From Figures 3 and 4, it is clear that the atoms are being redistributed over a larger height interval, a finding which is consistent with a reduced average number density. Qualitatively, such a swelling has been observed experimentally[52,53] during bombardment of aluminum surfaces with rare gas ions, where it was attributed to the accumulation of vacancy clusters below the surface.

In order to investigate the sputter removal process in more detail, it is of interest to determine the depth from which the sputtered material originates. A close inspection reveals that the ~5 ML of material removed during the first 200 impacts does not simply originate from the first five monolayers of the sample. Rather, Si atoms from many different original layers have been sputtered from the surface. Furthermore, the remaining Si atoms have been relocated vertically and are no longer in the height positions of their original layers. From the point of view of depth resolution, it is important to determine the contribution of atoms from each original layer to the sputtered yield. In Table 1, the fraction of atoms left in the sample that originate from the topmost layer is shown at different values of the fluence. Since these atoms are not removed, it is valuable to determine their new height coordinates and plot these distributions as a function of fluence. In order to do so, we bin the height values into slots of one monolayer thickness and assign a new layer index to each relocated atom. Initially, all of the atoms are located in layers below the original surface. However, as the accumulation of impacts increases, atoms may move into layers above the surface. Therefore, layers above the surface are defined with the same height limits and negative index values, whereas the indices of new layers corresponding to the original layers below the surface are positive. For different fluences, the fraction of remaining Si atoms originally located in the i-th layer but currently present in a new layer (k) is determined, and the resulting distribution is normalized by dividing the fractions in each set by the maximum value. As an example, the distributions of vertical positions of atoms originally located in the first layer are shown as plots of the normalized fraction of atoms vs the new layer index (k) in Figure 6. As the fluence increases, the distributions shift to a greater fraction at higher layers and the curves broaden. From these curves, it can be seen that the vertical positions of the Si atoms are relocated and there is a significant change in depth. The curves extend up to ten layers above the original surface and exhibit a tail into the layers beneath the original surface. The half-width of the distribution shown by the heavy dark line increases with fluence and is equal to ~15 layers after 200 impacts. Similar distributions were calculated for atoms originating from each of the top ten layers and are used in corrections for vertical mixing in the statistical sputtering model discussed in the next section.

It also constructive to determine how the fraction of Si atoms remaining from the ith original layer decreases as a function of fluence. In order to normalize the resulting curves with respect to variable parameters like the sputter yield, layer thickness or sample density, the number of monolayer equivalents removed as a function of fluence is calculated, and these values are used instead of the fluence for the x axis. In Figure 7a, the fraction of Si atoms remaining from each of the ten topmost original layers is plotted as a function of the number of monolayer equivalents removed. These distributions are important with respect to sputter depth profiling, because they reveal how the surface is being eroded by the C_{60} projectile bombardment. Ideally, one would want a "layer-by-layer" removal, where the uppermost surface layer is completely removed before the second layer starts to be depleted etc. It is evident that such a removal mechanism would result in optimum depth resolution.

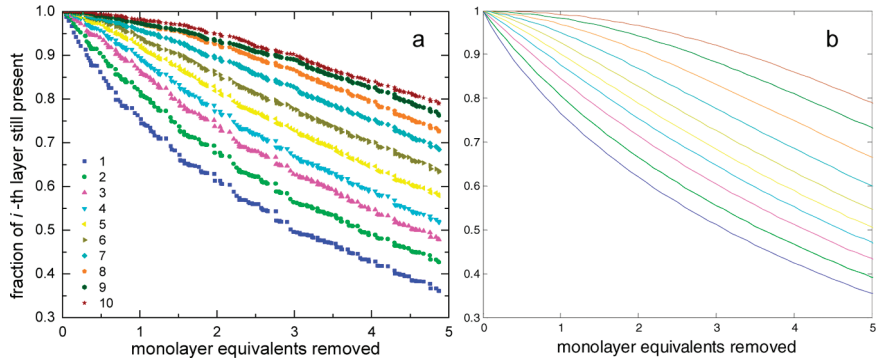

Figure 7. Fraction of atoms originally located in the i-th layer that are still present somewhere in the sample vs number of monolayer equivalents removed by sputtering. (a) Results from MD simulations and (b) corresponding plots predicted by the statistical sputtering model. The color coding of the layers is defined in the text and is illustrated in Figure 1b. The same color coding will be used in Figures 8−11.

TABLE 2: Parameters c_j and D_j Entering the Statistical Sputtering Model As a Function of Layer Depth (j) beneath the Momentary Surface[a]

layer	1	2	3	4	5	6	7	8	9	10
c_i	0.34	0.23	0.15	0.10	0.07	0.04	0.03	0.02	0.01	0
D_j	3.5	4.7	5.7	5.2	3.1	1.9	1.3	1.5	1.5	1.2

[a] The values have been derived from the MD data as described in the text. c_j: fraction of sputtered atoms originating from the jth layer; D_j: diffusivity constant at layer (j).

The data presented in Figure 7a, however, clearly demonstrate that this is not the case. Even after removal of 5 ML from the surface, about 36% of the original surface layer is still present, with the atoms being spread over almost 30 monolayers. On the other hand, layers below the surface immediately start to become depleted upon the beginning of bombardment, even though they are still covered and buried prior to the projectile impact. This observation reflects the depth-of-origin distribution of the sputtered material. Apparently, a C_{60} cluster impact onto the virgin surface removes atoms not only from the uppermost but also simultaneously from deeper layers. Under the conditions applied here, only about 34% of the sputtered atoms originate from the uppermost surface layer, and about 10% originate from depths beneath the fifth layer (see Table 2). Note that this finding is markedly different from what is generally observed under atomic ion bombardment, where more than 90% of the sputtered material originates from the uppermost surface layer.[54]

As fluence accumulates and more and more material is sputtered, deeper layers become exposed to the ion bombardment. At the same time, atoms from deeper layers become relocated and may move toward the surface, where they are more efficiently removed. This leads to the characteristic shape of the curves in Figure 7, where deeper layers initially start with a horizontal tangent and then become sequentially depleted. This qualitative behavior is easy to explain and will be discussed in more detail below. In fact, the curves displayed in Figure 7a represent important output of the MD simulations which will be compared to the predictions of the statistical sputtering model below.

3. Statistical Sputtering Model

In this section, we utilize a simple model describing the statistical nature of the sputtering process under cluster bombardment. The model is based on the division of the sample into monolayers (i) of thickness $d_{\text{layer}} = n^{-1/3}$ containing $N_{\text{layer}} = n^{2/3}$ atoms per unit area with n being the volume density of atoms. It should be noted that the model formulation remains the same for arbitrary values of d_{layer} provided the value of N_{layer} is changed accordingly. Originally, the index (i) runs from 1 to ∞ with $i = 1$ denoting the uppermost layer of the virgin surface. The goal is to follow the fate of atoms originating from different layers with respect to both their vertical motion in the sample and their removal by sputtering as a function of the projectile ion fluence. For that purpose, we introduce a filling factor θ_i defined as the fraction of atoms that are still present in the ith layer. In principle, this quantity can assume values between 0 and 1, where $\theta = 1$ denotes a completely filled layer with N_{layer} atoms per unit area. Upon start of the projectile ion bombardment, the different layers are becoming sequentially depleted and the momentary surface starts to recede due to sputter erosion. In the frame of the model, this process is described by a temporal change of the θ_i values from their initial values of $\theta_i = 1$ at the beginning to $\theta_i = 0$ at infinite fluence.

a. Model Description. Let us start with the assumption that atoms cannot move between different layers. In this case, θ_i can only be changed by sputter removal of atoms from that layer. The total number of atoms removed per impact is given by the sputter yield Y. Since sputtered atoms can, in principle, originate from different depths beneath the surface, we introduce constants c_j describing the fraction of sputtered atoms among the sputter yield which originate from the jth layer below the momentary surface, where $j = 1$ denotes the uppermost surface layer and particle conservation requires the set of c_j to be normalized as $\sum_j c_j = 1$.

Looking at a specific lateral site at the bombarded surface, the probability of that site being not occupied by an atom in the ith layer is $(1 - \theta_i)$. Therefore, the probability of layer (i) being the uppermost layer of the momentary surface at that site is given by $\prod_{k=1}^{i-1}(1 - \theta_k)$. In general, the probability of (i) being the jth layer beneath the momentary surface is then given by

$$p_i^{(j)} = \sum \{ \prod_{k=1}^{i-j} (1 - \theta_k) \prod_{k=i-j+1}^{i-1} \theta_k \} \qquad (1)$$

where the sum has to be taken over all possible combinations of $(j - 1)$ among the $(i - 1)$ layers above (i). Note that this probability is automatically normalized, i.e., $\sum_{j=1}^{i-1} p_i^{(j)} = 1$. Under these conditions, the number of atoms removed from the ith layer per projectile impact is given by $c_j \theta_i Y$, leading to a temporal variation of θ_i

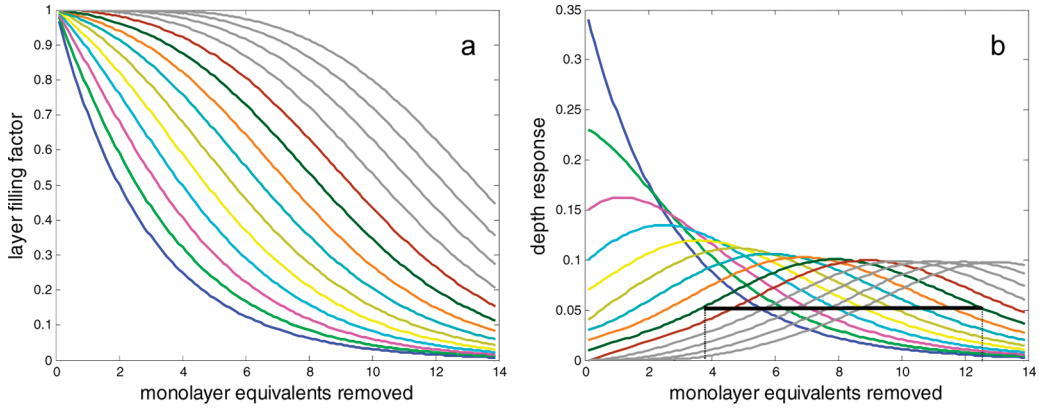

Figure 8. Filling factor θ_i of the ith monolayer (a) and derivative $d\theta_i/dx$ and (b) vs the number of removed monolayer equivalents x for $i = 1-14$ ($i = 1$ being the uppermost layer). The data were calculated from eq 4 without allowing for vertical motion of the atoms between different layers. The horizontal bar illustrates the half width (fwhm) of the distribution calculated for $i = 9$. (Color coding same as in Figure 10.)

$$\left.\frac{d\theta_i}{dt}\right|_j = -c_j\theta_i\frac{Yj_p}{N_{layer}} \tag{2}$$

In eq 2, j_p denotes the projectile ion flux density and $N_{layer} = n^{2/3}$ is the areal density of atoms within a layer. Summing over all possible j then yields the total change of θ as follows:

$$\frac{d\theta_i}{dt} = -\sum_{j\le i} p_i^{(j)}\left.\frac{d\theta_i}{dt}\right|_j \tag{3}$$

Substituting the number of removed monolayer equivalents $x = (Yj_p/N_{layer})\cdot t$ for the bombardment time t, the differential equation can be written as

$$\frac{d\theta_i}{dx} = -\sum_{j\le i} c_j\, p_i^{(j)}(x)\,\theta_i(x) \tag{4}$$

where $p_i^{(j)}(x)$ is the probability calculated from the set of θ_i using eq 1. Note that the rescaling from sputter time (t) or projectile ion fluence ($f = j_p t$) to removed material amount (x) eliminates the sputter yield as well as the atom density of the sample. Therefore, if either Y or N_{layer} (or both) change as a function of projectile fluence (which is likely to occur due to carbon implantation, surface topography development and defect formation), this change does not influence the form of eq 4 or all following equations. In fact, all plots of θ vs x which are shown below are invariant with respect to such changes.

In principle, the set of differential eqs 4 can be numerically solved provided the set of c_j are known. These parameters can, in turn, be taken from the MD results described in the previous section, by evaluating the number of sputtered atoms originating from different layers at the very beginning of the simulation. Averaging the respective data over the first ten impacts, we find the values depicted in Table 2. We assume these values to remain constant throughout the sputter removal process. At first glance, this assumption appears rather stringent. One should keep in mind, however, that the c_j represent fractions rather than total numbers of sputtered atoms. They are therefore not influenced by changes of the sputtering yield. Moreover, the statistical approach used here automatically includes the influence of surface topography on the composition of the sputtered flux by means of the probability distribution p as defined in eq 1. If a projectile impinges onto a corrugated surface, the momentary surface height exhibits a statistical distribution (see Figure 4) which results in an altered probability distribution $p_i^{(j)}$. In the frame of this statistical concept, it is therefore straightforward to calculate the contribution of a given layer (i) to the momentarily removed material increment dx by weighting a fixed, escape depth dependent fraction c_j with the probability $p_i^{(j)}$ of layer (i) to be located at a depth of (j) layers below the momentary surface. Summation of these contributions over all possible values of j then yields eq 4. Although we cannot a priori exclude possible changes of c_j with increasing number of removed monolayer equivalents x, we use constant values here as a first order approximation and compare the resulting SSM predictions to the MD simulation data. As will be shown below, we find rather convincing agreement which supports that assumption.

As explained above, it is of interest to look at the fraction of atoms originating from a particular layer that are still present somewhere in the sample after removal of x monolayer equivalents. Without any vertical motion of atoms, the θ_i data directly represent these fractions as well, because atoms cannot be removed from a layer except by sputtering. However, the MD data plotted in Figure 6 clearly demonstrates that bombardment induced motion of atoms between different layers of the sample must play a significant role. In the frame of the simple statistical treatment aimed at here, we include such motion by means of a diffusive approach. For that purpose, we introduce a bombardment induced hopping rate h for interchange of atoms between next-neighbored layers, leading to an additional term in eq 3 according to

$$\left.\frac{d\theta_i}{dt}\right|_{diff} = h(\theta_{i+1} + \theta_{i-1} - 2\theta_i) \tag{5}$$

In general, the hopping rate h will be depth dependent, leading to a different value h_j for each layer located at depth (j) beneath the momentary surface. Using the same scaling as above, we introduce a set of dimensionless diffusivity parameters $D_j = h_j Y j_p/N_{layer}$, leading to a modified version of eq 4

$$\frac{d\theta_i}{dx} = D_\uparrow(\theta_{i+1} - \theta_i) + D_\downarrow(\theta_{i-1} - \theta_i) - \sum_{j\le i} p_i^{(j)} c_j\theta_i \tag{6}$$

where

$$D_\uparrow = \frac{1}{2}(D_{i+1} + D_i) \quad \text{and} \quad D_\downarrow = \frac{1}{2}(D_i + D_{i-1}) \tag{7}$$

Note that the D values defined this way will in general depend on the erosion rate. While it is clear that bombardment induced particle mobility must scale with the projectile flux density j_p, this is not obvious for the sputter yield Y. In other words, if

hopping rate and sputter yield vary differently upon changing the bombarding conditions, the value of D will change accordingly. On the other hand, one might expect the diffusivity to scale with the deposited energy density in very much the same way as has been found for the sputter yield under cluster projectile bombardment,[44] hence rendering the definition according to eq 7 sensible.

It should also be noted that the diffusivity constants D_i entering eq 7 will change upon removal of layers located above (i). Using the same probability approach as for the sputter removal, we cast this variation into

$$D_i = \sum_{j \le i} p_i^{(j)} D_j \tag{8}$$

where D_j denotes the diffusivity value for a layer located at depth (j) beneath the momentary surface, which are introduced as a second set of input parameters besides c_j. Moreover, with regard to the data and discussion presented above (see Figure 6), it is necessary to allow for the possibility of atoms moving above the initial surface. In order to describe the vertical location of these "adatoms", we add a number of originally empty virtual layers above the initial surface with diffusion into and between these layers being treated in the same way as within the crystal. For the uppermost of these virtual layers as well as for the bottom layer of the system, we employ a Neumann boundary condition to prevent outward diffusion of atoms.

b. Results and Discussion. ***i. Dynamics without Mixing.*** For a system of 14 layers, the variation of θ_i calculated from eq 4 is shown in Figure 8. It is seen that the uppermost layer is exponentially depleted, as would be expected from eq 4 since $p_1^{(1)} = 1$. Under conditions where only the uppermost layer can contribute to the sputtered flux, θ_1 would fall to $1/e$ at $x = 1$. With the c_j distribution displayed in Table 2, its decay constant is reduced according to the value of c_1. In addition, deeper layers are initially also depleted with slopes reflecting their removal probabilities c_i and then become gradually exposed to stronger depletion as the amount of material removed above them increases. It is seen that about 50% of the 14th layer has been removed at $x = 14$, demonstrating the relatively good accuracy of the x-axis scaling. [This finding is important since eq 4 does not automatically ensure the normalization condition $\sum_i \mathrm{d}\theta_i/\mathrm{d}x = -1$, which must be required for consistency of the x axis.]

An important result of the statistical sputtering model, which is clearly visible in Figure 8, is the fact that a steady state is reached after removal of about ten ML of material. In this state, the layer removal process becomes stationary in the sense that the θ_i distribution is essentially reproduced by advancing both the layer index (i) and the number of removed monolayer equivalents (x) by one. This observation becomes even more evident if the derivative $\mathrm{d}\theta_i/\mathrm{d}x$ is plotted as shown in Figure 8b. These curves depict the amount of material that is being removed from the ith layer at a certain value of the accumulated projectile ion fluence, amount of removed material or eroded depth. At the same time, the data represent the contribution of atoms originating from that layer to the total sputtered flux. It is nicely seen that the fluence dependence of this quantity assumes a Gaussian-like distribution with half width $\Delta x_{\mathrm{fwhm}} \sim 9.3$ ML, which is advanced by $\Delta x \sim 1$ from layer to layer.

It should be noted at this point that the model presented here is based on the central assumption that the occupation probabilities θ_i entering $p_i^{(j)}$ are statistically independent. For completeness, it should be mentioned that different approaches describing the statistics of sputtering have been proposed in the literature where dependencies between the θ_i are assumed.[55,56]

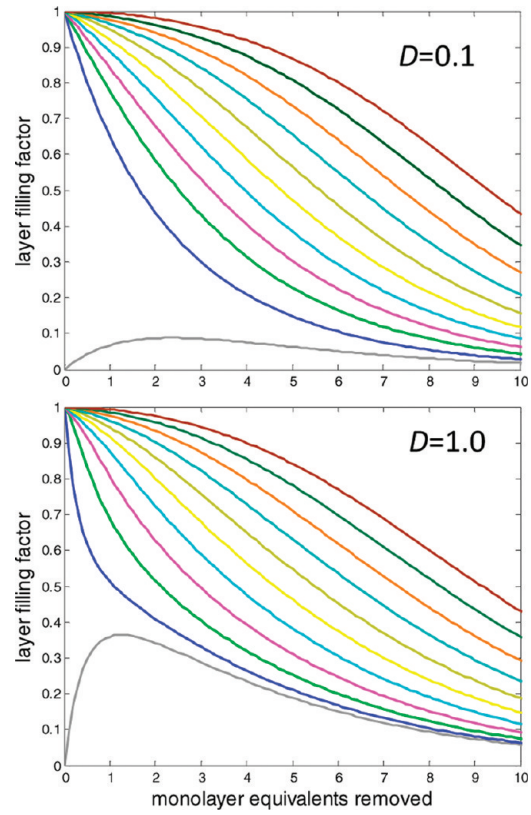

Figure 9. Filling factor θ_i of the ith layer vs the number of removed monolayer equivalents for different values of the diffusivity constant D (for definition of θ_i and D see text). The color coding is the same as in Figure 10 with the gray line indicating the data calculated for the virtual layer $i = -1$ located above the original surface.

In the particular case where only removal of atoms from the uppermost layer is considered (i.e., $c_1 = 1$, $c_{j>1} = 0$), a model based on such an approach has been introduced as the so-called "sequential layer model" of sputtering, which predicts Δx_{fwhm} to steadily increase with $\sqrt{x}$.[55] However, such an increase was not observed experimentally, ruling out the sequential layer model in this form.[57] In addition, it is not clear how such a model could be extended to arbitrary depth-of-origin distribution of the sputtered material, which is, however, necessary to describe the sputter removal under cluster ion bombardment.

ii. Inclusion of Mixing. As mentioned above, it is evident from the MD data that vertical motion of atoms between different layers must be included in the analysis. In order to get a feeling for the influence of the effect, results calculated for a system of 15 layers and constant values of $D = 0.1$ and $D = 1.0$ are presented in Figure 9. The variation of the filling factor θ_i is shown for the first ten surface layers of the sample ($i = 1-10$, same color code as before) plus one virtual layer located above the surface ($i = -1$, colored in gray). In comparison with Figure 8 (where $D = 0$), one finds the surface layers to be more rapidly depleted once diffusivity is switched on. This finding is easy to rationalize since atoms can move outward into the virtual layer, where they are being preferentially removed. The corresponding initial rise of θ_{-1} is clearly visible. It is seen that the model prediction qualitatively resembles the MD results plotted in Figure 8. A close inspection, however, reveals that the atoms appear to be removed much more rapidly than calculated by the MD simulation.

As a next step, it is necessary to determine the depth dependence of the diffusivity constants D_j. It is intuitively clear that the assumption of a constant D (independent of depth)

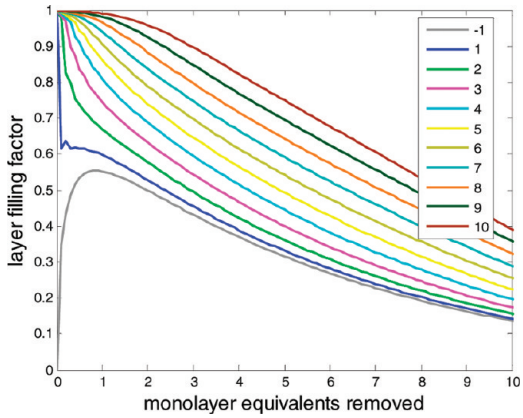

Figure 10. Filling factor θ_i of the ith layer vs the number of removed monolayer equivalents for a depth dependent diffusivity constant derived from the MD data.

cannot be sensible, since this quantity must be related to the energy deposition profile induced by the projectile impact and must therefore decay toward large values of j. On the other hand, it is relatively straightforward to determine depth dependent diffusion coefficients from the MD simulation data. Following the initial broadening of layer resolved height distributions such as that plotted for $i = 1$ in Figure 6, we find the half width to scale nicely with the square root of the projectile ion fluence as expected from a one-dimensional diffusive broadening of an original delta distribution. In terms of the scaling used above, atoms originally located in layer (i_0) will, after removal of x monolayer equivalents, be distributed between different layers (i) according to a Gaussian distribution

$$f(i) = \frac{1}{\sqrt{4\pi Dx}} \exp\left(\frac{(i - i_0)^2}{4Dx}\right) \tag{9}$$

Using the height distributions determined for different layers (i_0), the depth dependent diffusion constant can be extracted from the initial broadening by means of the half width (fwhm) determined after 50 impacts (corresponding to $x = 1.25$ ML) via

$$D(j = i_0) = \frac{(\text{fwhm})^2}{16x \ln 2} \tag{10}$$

The resulting values are displayed in Table 2. It is seen that the diffusivity goes through a maximum at a depth of about three layers below the surface and decays toward larger depths. Both trends are qualitatively expected from the deposited energy distribution.[41]

Figure 10 shows the fluence dependence of the filling factor θ_i is as calculated using the depth dependent diffusitivity values $D(j)$ taken from Table 2. Although a similar qualitative behavior is observed as in Figure 9b, there are quantitative differences resulting from the fact that (i) the surface-near diffusivity is relatively large and (ii) the diffusivity decreases with increasing distance from the momentary surface. Initially, the first layer is depleted very fast due to relocation of material above the initial surface. With increasing fluence, the depletion of deeper layers is turned on earlier due to the removal of material originally located above, thereby increasing the diffusitivity in these layers. It is apparent that the curves for subsequent layers still become approximately parallel and shifted by about one monolayer equivalent, indicating the establishment of a steady state after removal of about 10 momolayers.

In order to investigate the atomic motion in more detail and arrive at predictions that can be compared to the MD results, it is necessary to extend the model description by defining quantities $\theta_i^{i_0}$ denoting the monolayer fraction of atoms originating from layer (i_0) which have been relocated to layer (i) in the course of the ion bombardment. Based on the description of eq 6, the set of differential equations describing the variation of these quantities is given by

$$\frac{d\theta_i^{i_0}}{dx} = \sum_{j \le i} p_i^{(j)} \{D_\uparrow(\theta_{i+1}^{i_0} - \theta_i^{i_0}) + D_\downarrow(\theta_{i-1}^{i_0} - \theta_i^{i_0}) - c_j \theta_i^{i_0}\} \tag{11}$$

which via the normalization $\sum_{i_0} \theta_i^{i_0} = \theta_i$ yields eq 7 again. Looking at the i-distributions for a particular value of i_0 yields layer resolved height distributions which are found to describe the MD results quite well. Note that particularly for deeper layers, this finding is not trivial since these layers become gradually more exposed to the ion bombardment with increasing projectile fluence, thereby changing their effective diffusivity according to eq 8.

Summing $\theta_i^{i_0}$ over all layers (i) yields the fraction of atoms that were initially located in layer (i_0) and are still present in the sample. Using the diffusion coefficients of Table 2, the resulting fluence dependence of this fraction is plotted for $i_0 = 1-10$ in Figure 7b. These data can be directly compared with those extracted from the MD simulations shown in Figure 7a. It is seen that the overall variation predicted by the MD simulation is nicely reproduced by the model calculation. Note that in the form applied here the model contains no free parameters that need to be fitted to the MD curves. In contrast, all input parameters have been derived from other portions of the MD data itself, indicating that the statistical sputtering model is capable of reproducing essential features of the full MD simulations in a consistent manner. In view of its simplicity regarding the treatment of the depth-of-origin of the sputtered material and the bombardment induced mixing, we find this a remarkable observation.

iii. Discussion. The data that can be extracted from the statistical model calculations have significant implications for SIMS or SNMS sputter depth profiling experiments. As explained above, the depth resolution of such a technique is often evaluated using delta layer experiments, where thin analyte layers are embedded into a bulk matrix. Following the analyte signal as a function of projectile ion fluence or eroded depth then directly reveals the depth response function of the method, which is needed to deconvolute the measured signal transients in terms of actual depth distributions.

In principle, the layer removal distributions depicted in Figures 8b and 11 directly represent the predicted depth response function for a delta layer located at different depths (i). It should be noted that, although the distributions of Figure 11 could in principle also be extracted at least in part from the MD data shown in Figure 7a, it is obvious that the derivative of these curves is by far too noisy to obtain a meaningful result. As a first and important observation, we find that the width of these distributions, i.e., the depth resolution of the experiment, is largely determined by the statistical nature of the sputtering process. In fact, the value of Δx_{fwhm} extracted for, say, the ninth layer, is found to be significantly larger than that given by the depth-of-origin distribution of sputtered material, which can be evaluated from the set of c_j calculated by MD and amounts to 3−4 layers or 0.8−1.1 nm for the system studied here. Note that this value describes the information depth in static SIMS

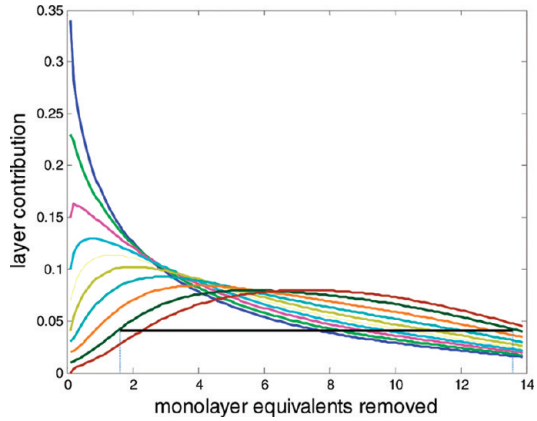

Figure 11. Contribution of atoms originally located in the *i*th layer to the sputtered flux vs number of removed monolayer equivalents. The horizontal bar illustrates the half width (fwhm) calculated for $i = 9$ (color coding same as in Figure 10 with the gray line indicating the data calculated for the virtual layer $i = -1$ located above the original surface).

or SNMS surface analysis. From $\Delta x_{fwhm} \approx 9$ ML determined from Figure 8b, it is evident that the sputter removal statistics contribute at least 5−6 layers or 1.3−1.6 nm to the observed depth resolution even under conditions where the vertical motion of particles within the sample is completely ignored. If bombardment induced mixing is included in the model, the response width is further broadened to $\Delta x_{fwhm} > 12$ ML, indicating that ion enhanced mobility contributes at least another 3 layers or 0.8 nm to the observed depth resolution. For the silicon sample studied here with a layer thickness of 0.27 nm, the resulting minimum depth response width is about 3.2 nm. Note that this value, which is solely determined by the statistical nature of sputter removal, decreases to about 1 nm under conditions where only removal from the uppermost layer needs to be considered and vertical motion is negligible. Such conditions can, for instance, be realized experimentally under bombardment with low-energy ions. For a molecular system with a typical density of 2.7 molecules/nm^3 and a corresponding monolayer thickness of about 0.7 nm, this results in minimum response widths on the order of 8−9 nm, which have indeed been observed in molecular depth profile experiments using C_{60} projectile ions.[10,19,25,26,58]

4. Conclusions

The accumulation of projectile fluence beyond the static limit bears great importance with respect to many applications of ion surface interaction phenomena. This is particularly true for sputter depth profiling experiments, where the surface is eroded by ion bombardment while the momentary surface composition is probed by means of a suitable analytical technique. Via their extension to multiple impact events, MD simulations can provide invaluable microscopic insight into the early stages of topography evaluation, surface roughening, etc. which may limit the depth resolution achievable by such a technique. Moreover, these simulations allow the assessment of fundamental issues such as the depth of origin of sputtered material as well as bombardment induced particle relocation. However, it is apparent that the MD simulations will not be able to explore the entire fluence regime needed to describe a real depth profiling experiment. As a consequence, it is necessary to find ways to extrapolate the results and findings obtained from the microscopic simulations toward higher fluences by means of simple phenomenological models, using the MD data to determine the essential model parameters. The present paper outlines a strategy in this direction by introducing a statistical sputtering model (SSM) which takes into account the statistical nature of the sputter removal of particles from a solid surface. The combination of microscopic MD simulations on one hand and the SSM model on the other hand is unique because it makes it possible to extrapolate the predictions of the MD simulations toward the regime of high projectile fluence. Using the MD data to determine its input parameters, we show that the model is capable of describing essential features of the ion surface interaction process including sputter removal and ion induced mixing by means of simple statistical concepts. In particular, it is shown that the model can reproduce the early stages of the depth response function measured in mass spectrometric techniques like SIMS or SNMS as calculated by MD. Using input parameters that are completely determined from the MD data, we find that the statistical nature of the sputtering process must contribute significantly to the depth resolution observed in such experiments. In particular, it is shown that the minimum width of the delta layer response function achievable under 20-keV C_{60} bombardment is limited to about 12 monolayers of the investigated sample. For the system studied here, this amounts to an optimum depth resolution of about 3 nm, while corresponding values on the order of 10 nm are predicted for molecular systems.

Acknowledgment. The authors are greatly indebted to Barbara Garrison, Mike Russo, and Zbigniew Postawa for their contributions to the development of the scheme used for modeling multi-impact bombardment, invaluable support regarding the MD simulations, and many enlightening discussions. We also thank Andreas Duvenbeck for his input regarding the statistical sputtering model. We acknowledge financial support from the Deutsche Forschungsgemeinschaft in the frame of the Sonderforschungsbereich 616 "Energy dissipation at surfaces". K.D.K also acknowledges financial support from a Faculty Research Grant from the College of Charleston as well as support for a sabbatical from the Department of Chemistry and Biochemistry at the College of Charleston. Computational support for the MD simulations was provided by the Graduate Education and Research Services (GEaRS) group of Academic Services and Emerging Technologies (ASET) at The Pennsylvania State University.

References and Notes

(1) Winograd, N. *Anal. Chem.* **2005**, *77*, 142A.
(2) Postawa, Z.; Czerwinski, B.; Szewczyk, M.; Smiley, E. J.; Winograd, N.; Garrison, B. J. *Anal. Chem.* **2003**, *75*, 4402.
(3) Weibel, D. E.; Wong, S.; Lockyer, N.; Blenkinsopp, P.; Hill, R.; Vickerman, J. C. *Anal. Chem.* **2003**, *75*, 1754.
(4) Wucher, A.; Sun, S.; Szakal, C.; Winograd, N. *Anal. Chem.* **2004**, *76*, 7234.
(5) Wucher, A.; Cheng, J.; Winograd, N. *Appl. Surf. Sci.* **2008**, *255*, 959.
(6) Zheng, L.; Wucher, A.; Winograd, N. *Anal. Chem.* **2008**, *80*, 7363.
(7) Zheng, L.; Wucher, A.; Winograd, N. *Appl. Surf. Sci.* **2008**, *255*, 816.
(8) Willingham, D.; Kucher, A.; Winograd, N. *Appl. Surf. Sci.* **2008**, *255*, 831.
(9) Zheng, L.; Wucher, A.; Winograd, N. *J. Am. Soc. Mass Spectrom.* **2007**, *19*, 96.
(10) Cheng, J.; Wucher, A.; Winograd, N. *J. Phys. Chem. B* **2006**, *110*, 8329.
(11) Cheng, J.; Winograd, N. *Anal. Chem.* **2005**, *77*, 3651.
(12) Mahoney, C.; Fahey, A.; Gillen, G. *Anal. Chem.* **2007**, *79*, 828.
(13) Mahoney, C.; Fahey, A.; Gillen, G.; Xu, C.; Batteas, J. *Anal. Chem.* **2007**, *79*, 837.
(14) Fahey, A.; Gillen, G.; Chi, P.; Mahoney, C. *Appl. Surf. Sci.* **2006**, *252*, 7312.

(15) Mahoney, C.; Gillen, G.; Fahey, A.; Zu, Ch.; Batteas, J. *Appl. Surf. Sci.* **2005**, *252*, 6502.
(16) Gillen, G.; Fahey, A. *Appl. Surf. Sci.* **2003**, *203*−*204*, 209.
(17) Gillen, G.; Lance, K.; Freibaum, B.; Lareau, R. T.; Bennett, J.; Chmara, F. *J. Vac. Sci. Technol.* **2001**, *19*, 568.
(18) Green, F. M.; Shard, A. G.; Gilmore, I. S.; Seah, M. P. *Anal. Chem.* **2009**, *81*, 75.
(19) Shard, A. G.; Green, F. M.; Brewer, P. J.; Seah, M. P.; Gilmore, I. S. *J. Phys. Chem. B* **2008**, *112*, 2596.
(20) Fletcher, J. S.; Conlan, X. A.; Lockyer, N.; Vickerman, J. C. *Appl. Surf. Sci.* **2006**, *252*, 6513.
(21) Weibel, D. E.; Lockyer, N.; Vickerman, J. C. *Appl. Surf. Sci.* **2004**, *231*−*232*, 146.
(22) Kozole, J.; Wucher, A.; Winograd, N. *Anal. Chem.* **2008**, *80*, 5293.
(23) Cramer, H. G.; Grehl, T.; Kollmer, F.; Moellers, R.; Niehuis, E.; Rading, D. *Appl. Surf. Sci.* **2008**, *255*, 966.
(24) Gillen, G.; Fahey, A.; Wagner, M.; Mahoney, C. *Appl. Surf. Sci.* **2006**, *252*, 6537.
(25) Wucher, A.; Cheng, J.; Zheng, L.; Winograd, N. *Anal. Bioanal-.Chem.* **2009**, *393*, 1835.
(26) Wucher, A.; Cheng, J.; Zheng, L.; Willingham, D.; Winograd, N. *Appl. Surf. Sci.* **2008**, *255*, 984.
(27) Wucher, A.; Cheng, J.; Winograd, N. *Anal. Chem.* **2007**, *79*, 5529.
(28) Fletcher, J. S.; Rabbani, S.; Henderson, A.; Blenkinsopp, P.; Thompson, S. P.; Lockyer, N. P.; Vickerman, J. C. *Anal. Chem.* **2008**, *80*, 9058.
(29) Fletcher, J. S.; Lockyer, N. P.; Vaidyanathan, S.; Vickerman, J. C. *Anal. Chem.* **2007**, *79*, 2199.
(30) Delcorte, A. *Appl. Surf. Sci.* **2008**, *255*, 954.
(31) Vandervorst, W. *Appl. Surf. Sci.* **2008**, *255*, 805.
(32) Gillen, G.; Batteas, J.; Michaels, C. A.; Chi, P.; Small, J.; Windsor, E.; Fahey, A.; Verkouteren, J.; Kim, K. J. *Appl. Surf. Sci.* **2006**, *252*, 6521.
(33) Gillen, G.; Walker, M.; Thompson, P.; Bennett, J. *J. Vac. Sci. Technol.* **2000**, *18*, 503.
(34) Sun, S.; Wucher, A.; Szakal, C.; Winograd, N. *Appl. Phys. Lett.* **2004**, *84*, 5177.
(35) Kollmer, F. *Appl. Surf. Sci.* **2004**, *231*−*2*, 153.
(36) Shard, A. G.; Brewer, P. J.; Green, F. M.; Gilmore, I. S. *Surf. Interface Anal.* **2007**, *39*, 294.
(37) Fisher, G. L.; Dickinson, M.; Bryan, S. R.; Moulder, J. *Appl. Surf. Sci.* **2008**, *255*, 819.
(38) Krantzman, K. D.; Kingsbury, D. B.; Garrison, B. J. *Appl. Surf. Sci.* **2006**, *252*, 6463.
(39) Krantzman, K. D.; Kingsbury, D. B.; Garrison, B. J. *Nucl. Instrum. Methods B* **2007**, *255*, 238.
(40) Krantzman, K. D.; Webb, R. P.; Garrison, B. J. *Appl. Surf. Sci.* **2008**, *255*, 837.
(41) Krantzman, K. D.; Garrison, B. J. *Nucl. Instrum. Methods B* **2009**, *267*, 652.
(42) Krantzman, K. D.; Garrison, B. J. *J. Phys. Chem. C* **2009**, *113*, 3239.
(43) Russo, M. F.; Postawa, Z.; Garrison, B. J. *J. Phys. Chem. C* **2009**, *113*, 3270.
(44) Russo, M. F., Jr.; Garrison, B. *J. Anal. Chem.* **2006**, *78*, 7206.
(45) Ryan, K. E.; Russo, M. F., Jr.; Smiley, E. J.; Postawa, Z.; Garrison, B. J. *Appl.Surf. Sci.* **2008**, *255*, 893.
(46) Garrison, B. J. In *ToF-SIMS: Surface Analysis by Mass Spectrometry*; Vickerman, J. C., Briggs, D., Eds.; IM Publications and Surface Spectra Limited: Chichester, U.K., 2001; p 223.
(47) Garrison, B. J.; Postawa, Z. *Mass Spectrom. Rev.* **2008**, *27*, 289.
(48) Tersoff, J. *Phys. Rev. B* **1989**, *39*, 5566.
(49) Ziegler, J.; Biersack, J.; Littmark, U. *The stopping and range of ions in solids*; Pergamon Press: New York, 1985.
(50) Belko, V.; Posselt, M.; Chagarov, E. *Nucl. Instrum. Methods B* **2003**, *202*, 18.
(51) Postawa, Z.; Ludwig, K.; Piaskowy, J.; Krantzman, K. D.; Winograd, N.; Garrison, B. J. *Nucl. Instrum. Methods B* **2003**, *202*, 168.
(52) Petersen, A.; Busse, C.; Polop, C.; Linke, U.; Michely, T. *Phys. Rev. B* **2003**, 68.
(53) Busse, C.; Hansen, H.; Linke, U.; Michely, T. *Phys. Rev. Lett.* **2000**, *85*, 326.
(54) Harrison, D. E., Jr. *Crit. Rev. Solid State Matter Sci.* **1988**, *14*, S1.
(55) Hofmann, S. *Appl. Phys.* **1976**, *9*, 59.
(56) Seah, M. P.; Sanz, J. M.; Hofmann, S. *Thin Solid Films* **1981**, *81*, 239.
(57) Wittmaack, K.; Schulz, F. *Thin Solid Films* **1978**, *52*, 259.
(58) Wucher, A.; Cheng, J.; Winograd, N. *J. Phys. Chem. C* **2008**, *112*, 16550.

JP906050F